





Small Visible Defect Detection of Small Sample based on the Fusion of Multiple Features

Zhichao Sun¹  and Xiangzhi Wei² 

¹Shanghai Jiao Tong University, sunzhichao@sjtu.edu.cn

²Shanghai Jiao Tong University, antonwei@sjtu.edu.cn

Corresponding author: Xiangzhi Wei, antonwei@sjtu.edu.cn

Abstract. Small visible defects on the surfaces of products affect their appearance and sales. Machine vision is a common and effective detection method for detecting the defects. At present, visual detection based on deep learning has made a great breakthrough in terms of accuracy. However, this method is not suitable for the production of small-scaled products since it relies on a large amount of data to become effective and the training of the deep learning model usually requires a very long time. Typically, the production of a new design is limited to a small scale, and the initial sample is not sufficient for the evaluation function to predict small visible defects. To address this issue, a fast approach for small visible defect detection is developed based on a fusion of multiple features using a small sample of data, also a recursive scheme is developed to tune the coefficients of the evaluation function as the sample size increases during the production process. To validate the proposed approach, a set of experiments using a patch of 500 watch dials and 500 jewelry accessories were conducted. It is shown that this method can effectively improve the prediction accuracy of the evaluation function.

Keywords: Machine vision, Defect detection, Small sample, Rapid detection.

DOI: <https://doi.org/10.14733/cadaps.2022.924-935>

1 INTRODUCTION

Small visible defects often appear on the surface of products during the manufacturing processes. Visible defects directly affect the sales of the products, especially for those items that are worn on human bodies (e.g., watches and jewelry accessories). At present, a common detection method is manual detection, which may lead to problems such as low detection accuracy, low efficiency, and high labor intensity of workers. Therefore, it is of practical significance to realize the automatic or semi-automatic detection of visible defects on the surface of small parts of small scale.

Noncontact detection is widely used in the detection of surface defects of various products. The main technologies include eddy current detection [9,22,25], ultrasonic detection [6], radiographic detection [8], etc., but these methods are time-intensive and inefficient [18]. With the rapid development of computer vision technology, visual inspection has been widely used because of its

advantages of fast, high precision and noncontact. For example, Shanmugamani et al. [21] extracted texture features based on histogram and gray-level co-occurrence matrix from the segmented image for classification; Dubey et al. [7] analyzed the geometric features of the region and identified the defects by using the maximally stable extremal region technique; Anandan et al. [1] transformed the input image into the frequency domain and detected defects by analyzing the frequency feature; Li et al. [14] extracted Histogram of Oriented Gradient (HOG) features and used classification algorithm to identify workpiece defects.

The above detection method requires a high degree of matching between features and defects. However, whether a defect is visible or not relies on people's subjective judgment, therefore it is difficult to objectively and effectively analyze the features of defects.

In recent years, with the development of deep learning, defect detection based on deep learning have attracted more and more attention [11]. Using deep learning can effectively extract high-dimensional information in the image, which avoids the cumbersome image processing steps of traditional methods. Wei et al. [23] used deep neural network to detect and identify defects of parts and achieved a high recognition accuracy. Mei et al. [16] reconstructed image patches with convolutional denoising auto-encoder networks at different Gaussian pyramid levels, and synthesized detection results from these different resolution channels to generate final detection results. Maestro-Watson et al. [15] proposed a U-NET-based Full Convolutional Neural Network for semantic segmentation of surface defects. Chen et al. [4] proposed a convolutional neural network (CNN) and Naive Bayes data fusion scheme to detect crack defects in a single video frame. Yang [24] proposed a Feature Pyramid and Hierarchical Boosting Network (FPHBN) for crack detection. Chen et al. [5] used deep convolutional neural network to locate and extract defects. Park et al. [17] detected scratches and other defects on the surface of parts by building several types of deep networks of different depths and layer nodes to select adequate structures. Ren et al. [19] used features transferred from a pre-trained deep learning network to obtain pixel-level prediction through convolution of input images.

But using deep learning method requires a large amount of data to become effective. Typically, the production of a new design is limited to a small scale, and the initial sample is not sufficient to implement the deep learning method. In the actual production process, it is difficult to obtain enough defect samples due to the low production error rate. In addition, the training of the deep learning model also requires a very long time.

In this paper, we proposed a fast detection method based on a small sample of data. The accuracy of our approach is guaranteed by using a fusion of multiple features of the defects. To further improve the accuracy of our approach, based on the initial evaluation function derived from the origin small set of data, we develop a self-learning mechanism to recursively tune the coefficients of the evaluation function, which is achieved by adjusting the coefficients of the function by using the prediction accuracy of new products.

The main contributions of this paper include the following aspects: The statistical analysis method is used to quickly analyze a small amount of data and obtain the initial evaluation function, which can shorten the development cycle. The fusion analysis of multiple features ensures the accuracy of defect description. In the production process, the recursive tuning method is used to continuously optimize the initial evaluation model. This makes the predictive power of the evaluation model continuously enhanced. And this method can effectively prevent over-fitting, improve the evaluation accuracy and robustness. This advantage is particularly suitable for the defect detection of actual industrial productions.

The remainder of the paper is organized as follows: Section 2 presents our proposed methodology, Section 3 validates our approach with a set of experimental results, and finally Section 4 concludes the paper with some discussion.

2 METHODOLOGY

This paper takes the dial of a watch as an example to illustrate our method. However, our method is also applicable to the other products. There are visible defects and invisible defects on the surface of a dial (Figure. 1). In practice, invisible defects do not affect the appearance and the sale of the product, and thus invisible defects are allowed in qualified products. Visible defects will directly affect the appearance of the product, so it is necessary to detect visible defects in the production process.

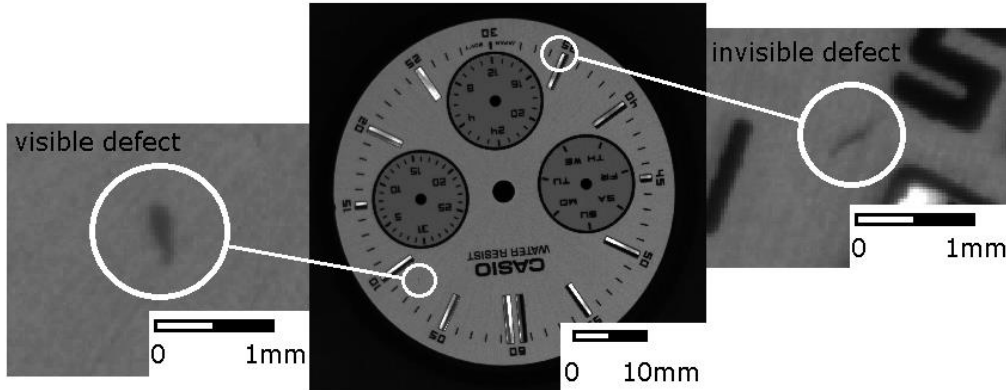


Figure 1: Visible and invisible defects on a dial.

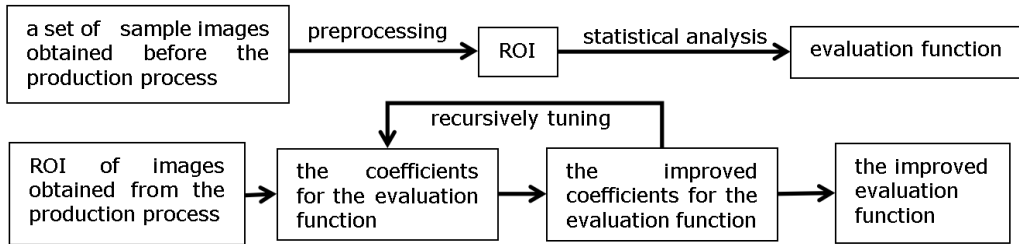


Figure 2: Flowchart of our approach.

Figure 2 shows the flow of our detection method:

1. Preprocessing the dial image to extract the ROI (Region of Interest, including visible and invisible defect regions).
2. A statistical analysis is performed on the ROI to establish the evaluation function
3. Using the new data obtained from the subsequent production process to recursively tune the coefficients of the evaluation function.

2.1 Preprocess

The role of preprocessing is to extract the ROI (Region of Interest, including small visible defect regions and invisible defect regions) of the dial image. Given a set of dial images and a standard dial image, we shall preprocess them as follows: (1) Extract the standard mask of the standard image; (2) match the standard mask and the dial image to mask the irrelevant regions of dial image, and then extract the ROI.

2.1.1 Extract the standard mask

To extract the standard mask (with irrelevant regions) of a standard image (free of defects), it is necessary to extract the boundary edges of the irrelevant region. Canny edge detection has been widely used to extract the edge because of its fast calculation speed and accurate edge location [3]. Therefore, in the paper, the Canny edge detection is used to extract the edge of the standard mask. The steps to extract the standard mask are as follows:

Step 1: Smoothing the input image.

A smoothed image can be obtained by performing a convolution operation on Gaussian function $G(x,y)$ and input image $f(x,y)$. The smoothed image $f_s(x,y)$ can be expressed as Equation (2.1).

$$f_s(x,y) = G(x,y) \cdot f(x,y) \quad (2.1)$$

Step 2: Calculate the modulus and gradient direction

Set $M(x,y)$ as the modulus of the gradient, $\theta(x,y)$ is the gradient direction and the expression is as shown in Equation (2.2).

$$\begin{cases} M(x,y) = \sqrt{g_x^2 + g_y^2} \\ \theta(x,y) = \arctan\left(\frac{g_x}{g_y}\right) \end{cases} \quad (2.2)$$

Where g_x and g_y are the first derivatives in the x and y directions, respectively. g_x and g_y are shown in Equation (2.3).

$$\begin{cases} g_x = [f_s(x+1,y) - f_s(x,y) + f_s(x+1,y+1) - f_s(x,y+1)] / 2 \\ g_y = [f_s(x,y+1) - f_s(x,y) + f_s(x+1,y+1) - f_s(x+1,y)] / 2 \end{cases} \quad (2.3)$$

Step 3: Non-maximum suppression

The global gradient is not sufficient to determine the boundary edges, and $M(x,y)$ needs to be refined by using non-maximum suppression to retain the local gradient maximum points, which ensure accurate edge positioning.

Step 4: Double threshold processing and connectivity analysis

Set a high threshold and a low threshold to extract edge pixels. First select the appropriate high threshold Th and low threshold Tl . If $M(x,y) \geq Th$, then the point is considered to be on the boundary edge, else otherwise. If $Tl \leq M(x,y) \leq Th$, then we need to judge whether there is any pixel in the neighborhood of the point that is greater than the high threshold Th . If so, then that point is the edge point. Finally, the resulting point is the edge point of the standard mask. The boundary edges of the standard mask of the standard image extracted is shown in Figure 3.

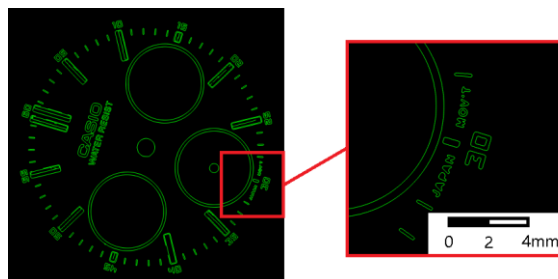


Figure 3: The boundary edges of a standard mask.

2.1.2 Covering irrelevant region

After obtaining the standard mask from a dial free of defects, we can remove the regions that do not require detection (metal parts, such as scales and marks) in the dial image. For this purpose, the standard mask and the dial image need to be matched. Figure 4 shows the main flow of covering the irrelevant regions.

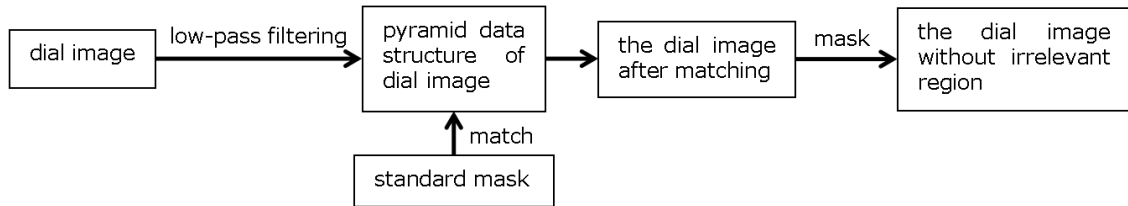


Figure 4: The main flow of covering the irrelevant region.

To reduce the matching time, we applied a pyramid search strategy [10] as follows. Build a pyramid data structure. The pyramid data structure consists of 4 images. The lowest level of the pyramid is the original dial image. Subsequently, the image of the upper layer is obtained from a lower layer by low-pass filtering, and its resolution is also lower.

When conducting the matching with the pyramid data structure, the standard mask is matched in a top-to-down fashion. In this process, the feature used for matching is the subpixel contour of edge. The Hausdorff distance is used to measure the matching rate. The closer the match, the smaller the Hausdorff distance value is. Suppose that the edge of the standard mask is composed of $A = a_1, \dots, a_p$, and the edge of the dial image is composed of $B = b_1, \dots, b_q$, then the Hausdorff distance is defined as Equation (2.4):

$$\begin{cases} H(A, B) = \max[h(A, B), h(B, A)] \\ h(A, B) = \max_{a \in A} (\min_{b \in B} \|a - b\|) \\ h(B, A) = \max_{b \in B} (\min_{a \in A} \|b - a\|) \end{cases} \quad (2.4)$$

In the formula, $H(A, B)$ is called the two-way Hausdorff distance, which is the most basic form of Hausdorff distance. $h(A, B)$ and $h(B, A)$ are called one-way Hausdorff distance from set A to set B and from set B to set A , respectively [12].

Finally, the exact translation and rotation parameters of the standard mask relative to the dial image is obtained. And then we can use Equation (2.5) to transform the standard mask to the right position in the dial image [13].

$$\begin{bmatrix} u' \\ v' \\ 1 \end{bmatrix} = \begin{bmatrix} \cos \theta & -\sin \theta & 0 \\ \sin \theta & \cos \theta & 0 \\ 0 & 0 & 1 \end{bmatrix} \begin{bmatrix} 1 & 0 & x \\ 0 & 1 & y \\ 0 & 0 & 1 \end{bmatrix} \begin{bmatrix} u \\ v \\ 1 \end{bmatrix} \quad (2.5)$$

In the formula, (x, y, θ) is the translation and rotation parameters of the standard mask relative to the dial image. (u, v) is the coordinates of the pixel of the original standard mask, (u', v') is the coordinates of the pixel of the standard mask after the transformation.

Refer to Figure 5 for an example, the dial images of each layer and the matching results are shown. From left to right, the image resolution and the matching accuracy become higher.

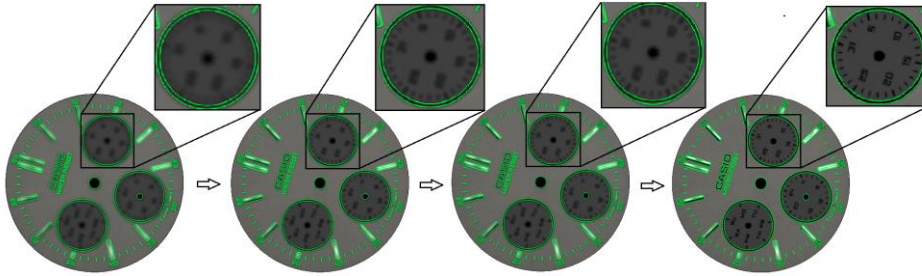


Figure 5: The process of matching, the green part of each image is the standard mask (transformed w.r.t the background image).

After the matching process, the standard mask can be used to mask the irrelevant regions of the image. Refer to Figure 6, it can be seen from the figure that the irrelevant regions of the dial image are masked (shown in dark).

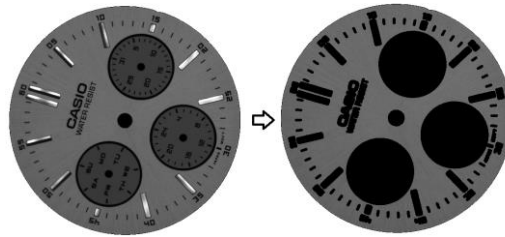


Figure 6: The effect of the mask operation, and dark regions in the right image indicate the masked regions that are not used for defect detection.

2.1.3 Extraction of the ROI

After masking the irrelevant regions of the dial image, the ROI can be extracted from the difference of image before and after the mean filtering, the calculation formula is Equation (2.6).

$$D(x,y) = |g(x,y) - f(x,y)| \quad (2.6)$$

In the formula, $D(x,y)$ is ROI. $f(x,y)$ is the image before mean filtering, $g(x,y)$ is the image after mean filtering.

After the above processing, the ROI is extracted and part of ROI is shown in the Figure 7. Note that the pixels of irrelevant region (scales and marks, etc) are set as 0 (black color), which makes the gray level of the defects w.r.t the remaining regions more significant.

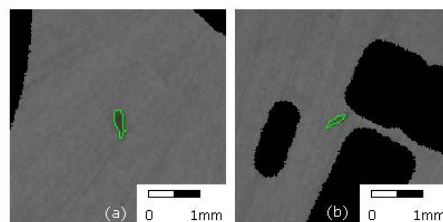


Figure 7: ROI: (a) a visible defect, (b) an invisible defect.

2.2 Statistical Analysis

After extracting the ROI, the multiple features of ROI is fused for statistical analysis to establish the evaluation function.

In this paper, multiple regression analysis is performed on the multiple features of ROI extracted (by using preprocessing) from 40 images (the images are from the initial sample images obtained before the production process) to establish the evaluation function. In the evaluation function, features is input and defect type is output. The steps are as follows:

2.2.1 Selection of features

In order to improve the capability of the evaluation model, several features are combined for analysis. The initially selected variables are F_i $i = 1, 2, 3, 4, 5$, which are defined as follows: Area F_1 is the area of a defect; Convexity $F_2 = F_0 / F_c$, where F_c is the convex hulled area of the region, and F_0 is the area of the region; Rectangularity $F_3 = A / A_r$, where A is the area of the region, and A_r is the area of the minimum enclosing rectangle of the region; length-width $F_4 = L_l / L_w$, where L_l and L_w are the length and width of the minimum enclosing rectangle of the region, respectively. Compactness $F_5 = \max\{1, e^2 / 4\pi F_1\}$, where e is the peripheral length of the defect region. However, the relationship among these variables is unknown. Therefore, these variables should be further screened to distinguish the significant ones.

2.2.2 Determination of defect types

In the evaluation function, the defect type (visible or invisible) is the output of the function. Therefore, when building the evaluation function, we also need to manually determine the type of defect which is used to generate the evaluation function.

The method to manually determine the type of defect is as follows: Three inspectors with normal vision are assigned the same set of defect samples with the 40 images. For the same suspect region, if two or more inspectors think the region is a visible defect, the region can be regarded as a visible defect.

2.2.3 Establishment of evaluation function

We use the stepwise regression method to further screen the variables. The idea of stepwise regression is to add the variables one by one. We use the F-test ($p < 0.1$) to judge whether a variable is significant. With the above processing, only F_1 , F_2 , F_1^2 and F_2^2 are significant.

The least square method was used to calculate the coefficients in the evaluation function, and the software Minitab 19 (Minitab Inc., USA, version 19.2-64 bit) was used for calculation.

The evaluation function can be expressed in Equation (2.7).

$$Y = 0.02527F_1 - 17F_2 - 0.000103F_1^2 + 9.82F_2^2 + 6.88 \quad (2.7)$$

In the equation, where Y is the evaluation value. If the response value $Y > 0.5$, the region is considered to be a visible defect, else otherwise.

In addition, the accuracy of the evaluation function can be evaluated by Equation (2.8).

$$R^2 = 1 - \frac{\sum (Y_{actual} - Y_{predict})^2}{\sum (Y_{actual} - Y_{mean})^2} \quad (2.8)$$

A high value of R^2 indicates a strong correlation between the variables and the value of Y .

2.3 Recursive Tuning

The original evaluation function can be further optimized by tuning the coefficients using the new data obtained from the subsequent production process. More precisely, in Equation (2.7), the coefficient $k_1 = 0.02527$, $k_2 = -17$, $k_3 = -0.000103$, $k_4 = 9.82$, and $k_5 = 6.88$ need to be tuned.

The method of recursively tuning is used to optimize the evaluation function. The main idea is that after the original evaluation function is obtained, the original evaluation function can be used to detect the defects in images during the production process. At the same time, the coefficients are tuned by using new data. When the evaluation function is optimized to a user-defined target, the recursively tuning optimization process is completed.

According to each region r extracted (during the preprocessing) from 50 images (the images were taken from the production process), we shall calculate its correction value (Equation (2.7)) by following steps:

To evaluate the difference between the evaluated value (Equation (2.7)) and the actual value (1 or 0, visible or not, observed by the users), we define the loss function in Equation (2.9).

$$Cost^r = \frac{1}{2} [\sigma(Y^{(r)}) - Y^{(r)*}]^2 \quad (2.9)$$

where $Y^{(r)}$ is calculated from Equation (2.7), $Y^{(r)*}$ is the actual value of region r . $\sigma(x)$ is the activation function for transforming the value of $Y^{(r)}$ into a range of $[0, 1]$ (since the value of $Y^{(r)*}$ is either 0 or 1), and can be expressed in Equation (2.10).

$$\sigma(x) = \frac{1}{1 + e^{-x+0.5}} \quad (2.10)$$

By taking the partial derivative of the loss function, the correction value $\Delta k_m^{(r)}$ ($m = 1, 2, 3, 4, 5$) of the value $k_m^{(r)}$ can be calculated in Equation (2.11).

$$\Delta k_m^{(r)} = -\eta \frac{\partial Cost}{\partial k_m} = -\eta \frac{\partial Cost}{\partial \sigma(Y)} \cdot \frac{\partial \sigma(Y)}{\partial Y} \cdot \frac{\partial Y}{\partial k_m} = -\eta (\sigma(Y) - Y^*) \cdot \sigma'(Y) \cdot V_k \quad (2.11)$$

where η is the step size, V_k is the values of variables.

The correction value $\Delta k_m^{(r)}$ ($m = 1, 2, 3, 4, 5$) is calculated from a single region r . However, the correction value of a single region cannot reflect the characteristics of all regions, and therefore we use the average of the correction values of all regions for this purpose. More precisely, we calculate the actual correction value Δk_m ($m = 1, 2, 3, 4, 5$), which is the average of the correction values of all regions extracted from 50 images, and its formula is shown in Equation (2.12).

$$\Delta k_m = \frac{\sum_{r=1}^n \Delta k_m^{(r)}}{n} \quad (2.12)$$

Therefore, the value of k_m in Equation (2.7) is updated by Equation (2.13).

$$k_m = k_m + \Delta k_m \quad (2.13)$$

The iteration process terminates as the change of loss between two iterations is less than a user-defined threshold (e.g., the change rate of loss is less than 0.001% for our case). Through 12 iterations on 50 images, the update evaluation function is obtained in Equation (2.14).

$$Y = 0.0252717F_1 - 17.00F_2 + 0.000159397F_1^2 + 9.82F_2^2 + 6.88 \quad (2.14)$$

3 EXPERIMENTAL ANALYSIS

In order to evaluate the accuracy of our method under the condition of small samples, we conduct experiments on 500 dials (Before that, 40 images were used to generate the evaluation function (Section 2.2) and 50 images were used to optimize the evaluation function (Section 2.3)). We also conduct experiments on 500 small jewelry accessories (Before that, 40 images were used to generate the evaluation function and 50 images were used to further tune the coefficients of the evaluation function). For all these products, their appearances significantly affect their sale, and therefore they require a fast defect detection during the production processes. Refer to Figure 8 for an example of the jewelry accessory, which is very common in China for girls to ornament their ears. Convolutional neural network (CNN) is a classic deep learning method, which is widely used in defect detection, image recognition and other fields [2,20]. We also compare our proposed method with CNN to further validate our approach. Particularly, in order to adapt the CNN model to the condition of small samples, we used Transfer Learning. The CNN model trained in this paper is a pre-trained CNN model, i.e., the CNN model has been trained on a large industrial image dataset and can serve as a good starting point for training our own model, based on which we further trained the CNN model with 40 sample images. The CNN and our method are used to predict the type of defects of the ROI (obtained by preprocessing). If all ROI of an image is correctly predicted, the image is considered correctly predicted. For fair comparison, the samples used in the training CNN model are the same as those used for generating the evaluation function in our method.

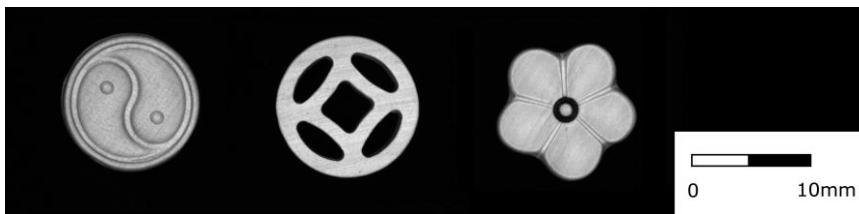


Figure 8: Jewelry accessory examples.

The HALCON 18.11 development kit was used to implement our algorithm. Hardware devices required for the experiment are a camera (HIKVISION MV-CE050-30UC) and a backlight (LOTS LTS-FT).

Table 1 summarizes the measurement accuracy and average measurement time of two types of parts by using two methods.

<i>Detected object and its corresponding method</i>	<i>accuracy(%)</i>	<i>time(ms)</i>
Dial (CNN)	86.6	292.204
Dial (Our method)	95.8	317.809
Jewelry accessory (CNN)	84.2	324.915
Jewelry accessory (Our method)	94.8	350.498

Table 1: Comparison of our method with CNN.

Figure 9-10 shows example images and their prediction results.

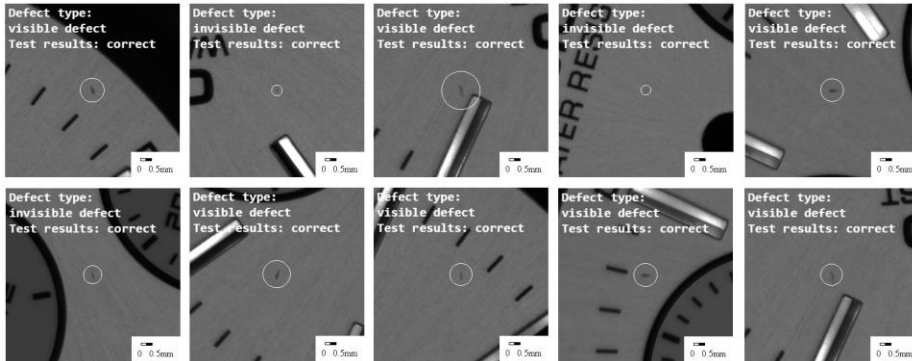


Figure 9: Results of example defect images of dial.

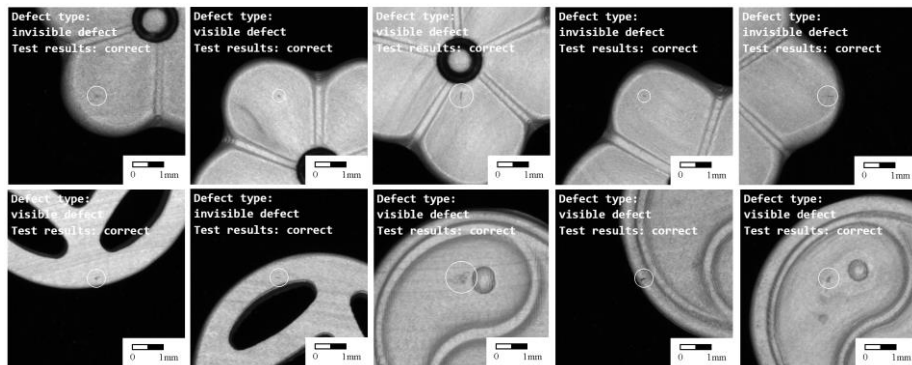


Figure 10: Results of example defect images of jewelry accessory.

It can be seen from the result that our method can detect the defects successfully. Moreover, in the case of such small samples, the accuracy of our method is better than the CNN method. Note that the accuracy can be further improved by using more data as the production goes on. From the perspective of average measurement time, there is not much difference between the two methods. The accuracy advantage of our method lies in the fuse of multiple features and the use of recursive tuning method: After the evaluation function is derived based on a small number of samples, it is then continuously refined by the fed data during the production process.

Our method has no fixed time of accomplishing a full cycle. It takes less time to generate the evaluation function in the early stage, the overall time of one full cycle mainly depends on the time of evaluation function optimization: The longer the optimization process is, the higher the detection accuracy will be. For CNN method, the early marking data, adjusting parameters of model and training model is very time-consuming, which makes it unsuitable for defect detection of small-scale products. In terms of the programming skills required by the user, our algorithm can be realized easily since it only involves a few critical math formulas (e.g., Equation (2.7) and Equation (2.14)). However, the method of CNN requires higher programming ability of users.

4 CONCLUSION

Fast visible defect detection is of critical importance for screening unqualified products. To ensure detection accuracy and shorten the development cycle, we proposed a method of generating

evaluation function based on a fuse of multiple features and a continuous tuning scheme for refining the evaluation function as the production goes on.

The experimental results show that our method can continuously optimize the evaluation function with small samples, and improve the evaluation accuracy. Compared with the CNN method, the detection accuracy of our method is higher under the same condition. In addition to the watch dial, we have shown that our method can also be extended to other applications. However, the initial evaluation of the truth still requires the intervention of users. How to automatically finish this efficiently is worthy of future research. In future research, we shall consider how to speed up the detection process with accuracy guarantee; and refine the approach of determining the evaluation function.

Acknowledgement:

This work is partially supported by the Science and Technology Commission of Shanghai Municipality Fund No. 18510745700.

Zhichao Sun, <https://orcid.org/0000-0003-4029-8844>

Xiangzhi Wei, <https://orcid.org/0000-0002-4541-0017>

REFERENCES

- [1] Anandan, P.; Sabeenian, R. S.: Fabric defect detection using discrete curvelet transform, *Procedia computer science*, 133, 2018, 1056-1065. <https://doi.org/10.1016/j.procs.2018.07.058>
- [2] Azizah, L. M. R.; Umayah, S. F.; Riyadi, S.; Damarjati, C.; Utama, N. A.: Deep learning implementation using convolutional neural network in mangosteen surface defect detection., *Computing and Engineering (ICCSCE)*, 2017, 242-246. <https://doi.org/10.1109/ICCSCE.2017.8284412>
- [3] Canny, J.F.: A computational approach to edge detection, *IEEE Transactions on Pattern Analysis and Machine*, 8(6), 1986, 679-698. <https://doi.org/10.1109/TPAMI.1986.4767851>
- [4] Chen, F. C.; Jahanshahi, R. M. R.: Nb-cnn: deep learning-based crack detection using convolutional neural network and naïve bayes data fusion, *IEEE Transactions on Industrial Electronics*, 65(99), 2018, 4392-4400. <https://doi.org/10.1109/TIE.2017.2764844>
- [5] Chen, J.; Liu, Z.; Wang, H.; Nunez, A.; Han, Z.: Automatic defect detection of fasteners on the catenary support device using deep convolutional neural network, *IEEE Transactions on Instrumentation and Measurement*, 67(2), 2017, 257-269. <https://doi.org/10.1109/TIM.2017.2775345>
- [6] Cruz, F. C.; Simas Filho, E. F.; Albuquerque, M. C. S.; Silva, I. C.; Farias, C. T. T.; Gouvêa, L. L.: Efficient feature selection for neural network based detection of flaws in steel welded joints using ultrasound testing, *Ultrasonics*, 73, 2017, 1-8. <https://doi.org/10.1016/j.ultras.2016.08.017>
- [7] Dubey, A. K.; Jaffery, Z. A.: Maximally stable extremal region marking-based railway track surface defect sensing, *IEEE Sensors Journal*, 16(24), 2016, 9047-9052. <https://doi.org/10.1109/JSEN.2016.2615333>
- [8] Zhang, Y.; Lefebvre, D.; Li, Q: Automatic detection of defects in tire radiographic images, *IEEE transactions on automation science and engineering*, 14(3), 2015, 1378-1386. <https://doi.org/10.1109/TASE.2015.2469594>
- [9] Gao, B.; Bai, L.; Woo, W. L.; Tian, G. Y.; Cheng, Y.: Automatic defect identification of eddy current pulsed thermography using single channel blind source separation, *IEEE Transactions on Instrumentation and Measurement*, 63(4), 2013, 913-922. <https://doi.org/10.1109/TIM.2013.2285789>

- [10] Grauman, K.: Pyramid match kernels: Discriminative classification with sets of image features, Computer Science and Artificial Intelligence Laboratory Technical Report, Tech, 2005, Rep. <https://doi.org/10.1109/ICCV.2005.239>
- [11] He, K.; Zhang, X.; Ren, S.; Sun, J.: Deep residual learning for image recognition, In Proceedings of the IEEE conference on computer vision and pattern recognition, 2016, 770-778. <https://doi.org/10.1109/CVPR.2016.90>
- [12] Lalonde; Marc; Beaulieu; Mario; Gagnon; Langis: Fast and robust optic disc detection using pyramidal decomposition and hausdorff-based template matching, IEEE transactions on medical imaging, 20(11), 2001. <https://doi.org/10.1109/42.963823>
- [13] Liang, T.; Qian, L.; Wenzheng, L.; Renjie, H.; Fayun, G.; Dongjie, Z.: Research and implementation of ceramic valve spool surface defect detection system based on region and multilevel optimisation, Nondestructive Testing and Evaluation, 34(4), 2019, 401-412. <https://doi.org/10.1080/10589759.2019.1623217>
- [14] Li, Y. B.; Li, B. L.; Xiong, Y.: Railway fastener state detection based on HOG feature, Transducer Microsyst. Technol, 32(10), 2013, 110-113. <https://doi.org/10.13873/j.1000-97872013.10.032>
- [15] Maestro-Watson, D.; Balzategui, J.; Eciolaza, L.; Arana-Arexolaleiba, N.: Deflectometric Data Segmentation Based on Fully Convolutional Neural Networks, International Society for Optics and Photonics: Mulhouse, 11172, 2019, 1117209. <https://doi.org/10.1117/12.2521740>
- [16] Mei, S.; Yang, H.; Yin, Z.: An unsupervised-learning-based approach for automated defect inspection on textured surfaces, IEEE Transactions on Instrumentation and Measurement, 67(6), 2018, 1266-1277. <https://doi.org/10.1109/TIM.2018.2795178>
- [17] Park, J. K.; Kwon, B. K.; Park, J. H.; Kang, D. J.: Machine learning-based imaging system for surface defect inspection, International Journal of Precision Engineering and Manufacturing-Green Technology, 3(3), 2016, 303-310. <https://doi.org/10.1007/s40684-016-0039-x>
- [18] Ph Papaelias, M.; Roberts, C.; Davis, C. L.: A review on non-destructive evaluation of rails: state-of-the-art and future development, Proceedings of the Institution of Mechanical Engineers, Part F: Journal of Rail and rapid transit, 222(4), 2008, 367-384. <https://doi.org/10.1243/09544097JRRT209>
- [19] Ren, R.; Hung, T.; Tan, K. C.: A generic deep-learning-based approach for automated surface inspection, IEEE transactions on cybernetics, 48(3), 2017, 929-940. <https://doi.org/10.1109/TCYB.2017.2668395>
- [20] Shang, L.; Yang, Q.; Wang, J.; Li, S.; Lei, W.: Detection of rail surface defects based on CNN image recognition and classification, In 2018 20th International Conference on Advanced Communication Technology (ICACT), 2018, 45-51. <https://doi.org/10.23919/ICACT.2018.8323642>
- [21] Shanmugamani, R.; Sadique, M.; Ramamoorthy, B.: Detection and classification of surface defects of gun barrels using computer vision and machine learning, Measurement, 60, 2015, 222-230. <https://doi.org/10.1016/j.measurement.2014.10.009>
- [22] Soni, A. K.; Rao, B. P.: Lock-in amplifier based eddy current instrument for detection of sub-surface defect in stainless steel plates, Sensing and Imaging, 19(1), 2018, 1-11. <https://doi.org/10.1007/s11220-018-0217-8>
- [23] Wei, X.; Yang, Z.; Liu, Y.; Wei, D.; Jia, L.; Li, Y.: Railway track fastener defect detection based on image processing and deep learning techniques: A comparative study, Engineering Applications of Artificial Intelligence, 80(APR.), 2019, 66-81. <https://doi.org/10.1016/j.engappai.2019.01.008>
- [24] Yang, F.; Zhang, L.; Yu, S.; Prokhorov, D.; Mei, X.; Ling, H.: Feature pyramid and hierarchical boosting network for pavement crack detection, IEEE Transactions on Intelligent Transportation Systems, 21(4), 2019, 1525-1535. <https://doi.org/10.1109/TITS.2019.2910595>
- [25] Yoshimura, W.; Tanaka, R.; Sasayama, T.; Enpuku, K.; Jensen, C. G.: Detection of slit defects on backside of steel plate using low-frequency eddy-current testing, IEEE Transactions on Magnetics, 54(11), 2018, 1-5. <https://doi.org/10.1109/TMAG.2018.2847729>